An experimental blade-controlled platform for the design of smart cross-flow propeller

Guillaume Fasse[a,*], Florent Becker[a], Frederic Hauville[a], Jacques-Andre Astolfi[a] and Gregory Germain[b]

[a]*Naval Academy Research Institute (IRENav), BCRM Brest, CC600, 29240 Brest Cedex9, France*
[b]*Ifremer, Marine Structure Laboratory 62200 Boulogne-sur-Mer, France*

Abstract

As an interesting alternative naval propeller, cycloidal propulsion offers a huge maneuverability to the vessel due to the ability to almost instantly orientate the thrust over 360°. While this system has been industrialized since the beginning of the 20th century by Voith-Schneider industries to supply low-speed ship (such as tug, buoyage boat, or some ferries), emergence of fast unmanned underwater vehicles renewed interest in this type of propulsion. Most ordinary cycloidal propellers use so far a mechanical system (gears, crankshaft-rod, belt-pulley) to control the blade rotation which restrains its use for a kinematic mode (epicycloidal or trochoidal) depending on the advance parameter.

As an academic technology platform, the French Naval Academy Research Institute (IRENav) developed a large-scale experimental cycloidal propeller (800kg, 0.4m radius) with the aim of testing and running diverse blade pitch laws in the quest for higher energy efficiency for both kinematic modes. Blades' pitching is here performed by servo-motors in order to control each blade independently. An embedded micro-controller sends pitch orders to speed controllers connected with each servo-motors.

The experimental blade-controlled platform is also instrumented with four fixed load sensors which measure global forces on the frame. An embedded 2D load-cell outfits one of the blade to measure local inflow hydrodynamic forces during the rotation. A torque sensor also measures the torque on the main shaft. This paper presents this experimental platform, capable of reproduce every imaginable kinematic motions, and widely instrumented to evaluate performances of cross-flow propeller.

Pitch regulation has been improved to obtain a sufficient quick response of auxiliary engines. However, pitch tracking validation shows a systemic error due the standard PID regulation loop used by speed controllers which depends essentially on the rotational speed and the considered pitch law (more sharp is the law and more the delay is high).

First in-water experiments have been performed at the IFREMER wave-current flume tank for a range of sinusoidal pitch laws to confirm the post process procedure and to determine performance curves for a range of advance parameters. Results show that depending on the advance parameter the more efficient law is different: more the advance parameter is high more the sinusoidal amplitude must be low for a better efficiency. These results confirm the requirement of an adaptable pitch control for cycloidal propeller to boost performances through different operating modes.

1. Introduction

For the last two decades, innovative naval propulsion systems have been investigated thanks to the growing development of unmanned underwater vehicles. Cross-flow propellers are promising alternative concepts from usual screw propellers. These systems take energy from unsteady hydrodynamic forces generated by blades oscillation or heaving like natural marine animal swimmers (bio-mimetism) [3, 27, 30].

Cross-flow propellers are characterized by the rotation of several blades around a main axis which is perpendicular to the freestream, as opposed to conventional screw propeller for which rotation axis is usually aligned with the freestream. The main rotation is associated with the oscillation of each blade around its own axis commonly called pitch rotation. The combination of these two rotations produces an unsteady hydrodynamic load which results on the thrust force (in the ship advance direction) and side force (perpendicular to the advance direction). Theses forces are varying along the main rotation angle, called orbital position θ, and highly depend on the running pitch law.

The main advantage of these propellers is to generate a 360° vectorial thrust force that significantly improves the ship's maneuverability. For this kind of propulsion, the advance parameter λ is defined as the ratio of the ship advance speed V_a to the rotational tip speed $V_r = \Omega R$ (where R is the vertical axis propeller radius) :

$$\lambda = \frac{V_a}{V_r} \tag{1}$$

Depending on its value two modes are distinguished by the blade kinematic which describes a cycloid path (cross-flow propeller is also referred as cycloidal propeller). Epicycloidal mode is defined for $\lambda < 1$: the rotational tip speed is higher than the ship advance speed. The blade leeding edge is hence mainly parallel to the tangent of the rotational tip speed to ensure that the relative kinematic velocity (vectorial sum of V_a and V_r) is coming from the leeding edge (and not from the trailing edge). Propellers using this kinematic mode are

*Corresponding author
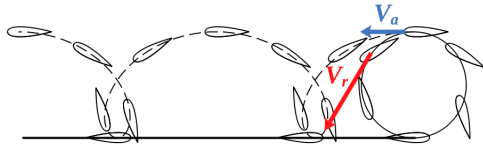ORCID(s):

referred as low-pitch systems.

Figure 1: Illustration of the epicycloidal path of one blade

On the other hand, trochoidal mode for $\lambda > 1$ allow the decrease of the rotational speed in comparison with the epicycloidal for a same advance speed. Because the advance speed is predominant in the expression of the kinematic relative velocity, the blade leeding edge is roughly aligned with the advance direction (see Figure 2). Decreasing the rotational speed has the main benefit to delaying the blades' cavitation. These propellers are referred as high-pitch systems.
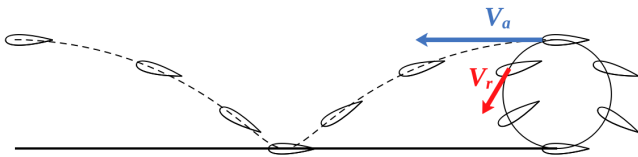

Figure 2: Illustration of the trochoidal path of one blade

Cross-flow propellers have been studied since 20th century beginning by Kirsten [19] with the dual scope of propeller and generator purposes with a fixed low-pitch mechanical system. Schneider [26] improved on Kirsten's propeller and partnered with Voith in 1928 to industrialize and commercialize their propeller renowned as the Voith-Schneider Propeller [4]. Since many experiments have been performed in Japan [29], in North America [6, 12, 14, 22, 24], and in Netherlands [20] to investigate this specific type of propulsion.
Meanwhile theoretical models has emerged to handle the complex flow description and predict the performance of these systems. In 1962, Taniguchi [29] has developed a quasi-steady method to numerically estimate the performance of epicycloidal propellers. His method was improved in 1981 by Zhu [31]. Sparenberg [28] proposed a theoretical model for single-blade propeller by minimizing kinematic energy in the wake. Mendenhall and Spangler [21] used a discrete-wake-vortex method to predict the behavior of a cycloidal propeller. Bose [5] adapted a multiple-streamtube-model from wind turbine theory to study high-pitch cycloidal propeller. Recent studies [9, 15] has implemented more complex models to continue to estimate as well as possible cycloidal propeller performance. Lastly improvements on modern CFD solvers are accurate validation resources and a new interesting area of work for optimization purpose [2, 10, 11, 17].

Cycloidal propellers blades are so far basically actuated by mechanical rotating technology (connecting rods, crank, camshaft, gears...) and then restrained to only one kinematic mode (epicycloidal or trochoidal). While low-pitch systems provide high thrust at very low ship speed (for harbour manoeuvring or dynamic positioning for example) they are lim-

ited in maximal ship speed (approximately 15knots for the Voith-Schneider Propeller). High-pitch systems can reach higher ship speed but are less efficient during starting phase. To take advantage of both modes, the IRENav interested in the design of an experimental cross-flow propeller with an electrical blade actuating. Three servo-motors enslaved by the main rotation are imposing independent blade movements. Blade control is no more limited by a mechanical system, all types of pitch law could be played. This allows to play pitch laws from both modes and to switch from one to the other mode during the rotation of the propeller.
Another interest is to play non-symmetric laws (from the two half of rotation disk point of view). Indeed, as mentioned by Roesler [24], since downstream blades pass through the wakes of upstream blades it is logical that optimal pitch law on the downstream half should be different than that on the upstream half. Physical phenomenon described by Halder [15] and resumed as dynamic virtual camber effects lead also to view the two half disk domains different for the generation of hydrodynamic loads.
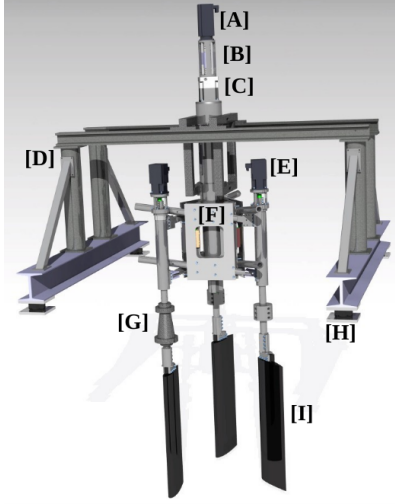This experimental cross-flow propeller is also instrumented with a blade-embedded load-cell, a torque sensor and encoders to measure time dependant hydrodynamic loads and angles during the rotation. The goal of this paper is to present this experimental system from a mechanical aspect and its blade control/command. Several pitch laws from both kinematic modes are tested and pitch track back is compared to the reference. Then experimental setup and post-process are described. Lastly preliminary measurements for sinusoidal pitch law are presented and discussed.

2. Experimental Propeller Design

The experimental transverse axis propeller presented here is an academic project driven by the French Naval Academy Institute in collaboration with IFREMER. The goal of this experimental blade-controlled platform is testing transverse axis systems pitch law for design or optimization purpose. In this article, the system is described as a propeller but it could also be used to test pitch law for marine energy converters (as it has originally been designed [8, 23]).

2.1. Mechanical Description

The experimental blade-controlled platform is named SHIVA for Intelligent Hydrodynamic System with Angle Variation. Figure 3 gives a Computer Aided Design (CAD) rendering of SHIVA and the main characteristics in the table (bold values highlight those used for the configuration of the presented results). SHIVA is a large experimental system (800kg, 2.5m high) composed of a steel triangular frame [F] connected to the main vertical driveshaft by a Morse taper and rotating through the fixed outer frame [D]. This outer frame is build from steel I-beams which ensures stability during the experiments. On the triangular frame three vertical shafts are assembled by sliding link to be able to move them far or toward the triangular frame center. These sliding guides are 7°-tilted to allow for an axisymmetric system, and to be

[A] Main Engine	Nominal Speed Ω_{main}	3000 [RPM]
	Nominal Power P_{main}	2500 [W]
[B] Torque Sensor	Measuring Range and Uncertainty (% of range)	± 20 [$N.m$] ; 0.5%
[C] Speed Reducer	Ratio	50
[D] Outer Frame	Total Weight	1000 [kg]
[E] Auxiliary Engines with Speed Reducer	Nominal Speed Ω_{aux}	1800 [RPM]
	Nominal Power P_{aux}	790 [W]
	Ratio	10
[F] Triangular Frame	Diameter ($D = 2R$)	**0.8** − 1.6 [m]
	Solidity ($\sigma = Nc/R$)	$0.5625 - 1.12/1.3 -$ **2.62**
[G] Blade load-cell	Measuring Range and Uncertainty	$F_{Nb} \pm 5000$ [N] ; 0.81%
		$F_{Tb} \pm 1000$ [N] ; 1.76%
[H] Fixed load-cells	Measuring Range and Uncertainty	$F_x \pm 5000$ [N] ; 0.8%
		$F_y \pm 5000$ [N] ; 0.22%
		F_z 7000 [N] ; 0.54%
[I] Blades	Number of blades N	3
	Blade chord (c)	0.15/**0.35** [m]
	Aspect Ratio ($AR = l/c$)	6.7/**2.8**
	Chord ratio ($c_r = c/R$)	$0.19 - 0.38/0.44 -$ **0.87**
	Blades cross section	NACA 0018

Figure 3: On the left is a CAD view of SHIVA and on the right is the table of characteristics (for sensors, percents are giving the uncertainty of the measure)

able to double the diameter to greatly modify the system solidity (for present experiments smallest diameter is chosen, D=0.8m). Radius of the propeller is defined as the distance between the center of the triangular frame and the center of each vertical secondary shafts. Three blades [I] are hooked up to each shaft and secured by bolts. Blades are made with filled stainless steel on a NACA0018 profile of 0.15m chord and 1m span. Blades can be wrapped by epoxy-fiberglass shell to increase the chord length at 0.35m. These shells also allow to change the blade profile and thus also modify the solidity of SHIVA. The solidity for the present experiments is 2.62.

The triangular frame is driven by the 2.5kW HRS115E6-130S (from SEM brand) main motor located at the top of the propeller [A]. A 50-ratio speed reducer [C] is used to increase the nominal torque and fit the rotational speed for our experiment values ($\sim$ 0-50 RPM). Each blade is also independently actuated by a 0.8kW HDM105C10-54S (from SEM brand) auxiliary motor [E] enslaved by the main rotation. A 10-ratio speed reducer is also used to adapt the motor rotational speed to the blade kinematic. Blades are rotating on their chord quarter which is the aerodynamic center for the NACA0018 airfoil.

Blades are rotating following the pitch law which is the expression of the angle β in function of the orbital angle θ. β is defined as the oriented angle between the ortho-radial line and blade chord. Another representation of the pitch is φ which is the oriented angle between the X-axis and blade chord. The latter definition is used for a simpler representation of the law in trochoidal mode because the blade is oscillating around the X-axis which corresponds to the advance direction (whereas it oscillates around the ortho-radial line for epicycloidal mode). These two pitch angles are related
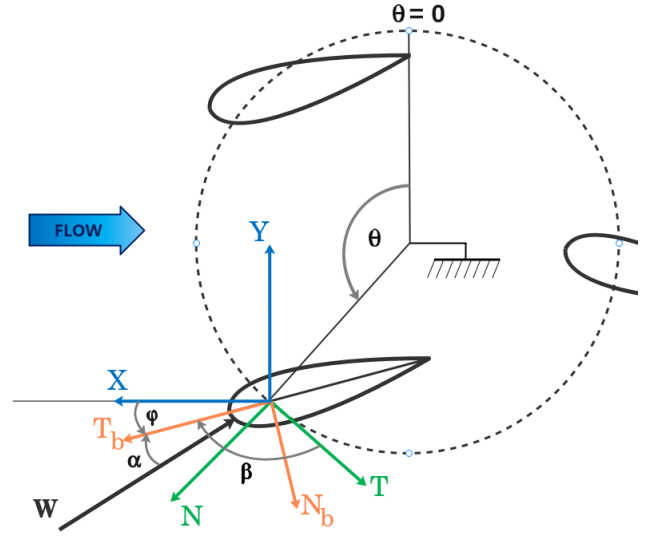
by the relation $\theta=\varphi-\beta$ (see Figure 4).

Figure 4: Representation of angles for an arbitrary position θ and an arbitrary relative velocity W

Pitch is directly related to the incidence α which is the angle between the blade chord and the local relative velocity W. Indeed, for cross-flow propellers, the aim is to orientate the blade during the rotation with the pitch angle in order to maximize the contribution of lift and drag forces, generated by the incidence α, that produces a thrust in the advance direction (X direction in this case). Pitch angle have a major impact on cross-flow propeller design because it also influences back hydrodynamic loads by affecting the flow inci-
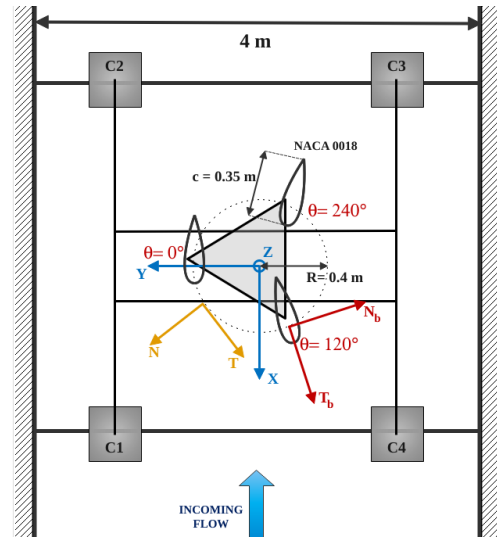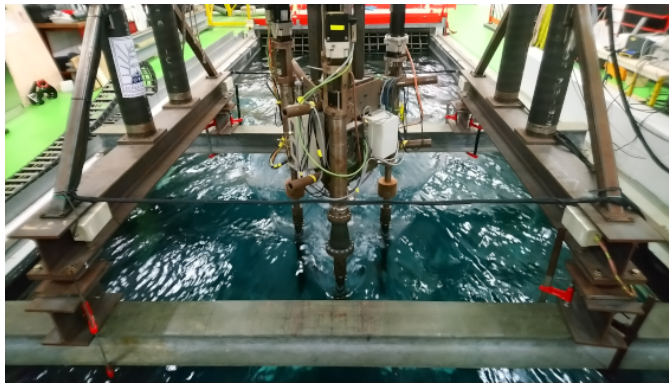
Figure 5: IFREMER wave and current flume tank overview

dence with the induced pitch velocity.

To carry out experiments, SHIVA is operating at the Boulogne-sur-Mer IFREMER wave and current flume tank which is 18 meters long by 4 meters wide and 2 meters depth (see Figure 5). Dimensions of SHIVA are suited for the IFREMER water tank to reduce hydrodynamic blockage effect. Indeed the ratio of the propeller frontal area divided by the tank section leads to a blockage of 15%. According previous study [7], the blockage effect overestimates hydrodynamic loads and efficiency for a ratio up to 50%. Here, these effects are thus neglected.

The fixed outer frame leans on two additional horizontal I-beams from IFREMER which elevate all the system just above the water: only the blades are under the water line of the tank (see Figure 3 and Figure 5). An alignment of the outer frame with the water tank guarantees that the flow direction is parallel to the outer frame. A mechanical adjustment of the 0°-position of the main rotation (corresponding to the triangular frame) and 0°-positions β_i of the three secondary motors are also done before every experiments to ensure that the incoming flow is also parallel to each 0°-positions β_i pitch blades (no incidence angle) for theta 0°-position. The flow velocity V is adjustable from 0.1 to 2.2 m/s, fixed to 1.2 m/s for this work, with a turbulence intensity of 1.5 %. Further information about IFREMER tank facilities are given by Gaurier [13, 18].

2.2. Measurement Instrumentation

SHIVA is instrumented with 4 fixed 3-components load-cells [H] located between the outer frame I-beams and IFRE-MER I-beams (see Figure 3). These load-cells provide global resulting solicitations of the propeller acting on the frame in the three directions **X**, **Y** and **Z** (see Figure 5). They measure loads for a range of $\pm 5000N$ in the X and Y direction and $+7000N$ in the Z direction (compression). Transfer matrix

and uncertainty are given by the supplier (Six-axes) and resumed in the table of the Figure 3.

One blade is instrumented with a 4-components load-cell [G] which measures local hydrodynamic loads in the direction of blade's chord **Tb** and normal to the blade **Nb** (see Figure 5). In-house calibration procedure was undertaken to determine matrix transfer to optimally reproduce the way the blade is stressed during experiments.

A torque sensor (4503B 020 L P0 00 KA2 from Kistler brand) is installed between the main motor and the main speed reducer [B] and measures the torque applied on the main drive-shaft with a measuring range between 0 and 20 N.m and an uncertainty of 0.5% of measuring range.

A CompactDAQ system from National Instruments (embedded NI cDaq-9184 linked with the stationary NI cDaq-9185) collects and synchronizes the data from all these measurement devices (embedded and fixed).

During the rotation, pitch angles β_i of each blade and orbital position θ are also recorded thanks to incremental rotary encoders with a 1024 pulse rate (8.KIS40.1362.1024 from Kübler brand) to provide both the real angle values (for projection of local forces into the global reference frame) and a feedback for the pitch control which is detailed in the next section. These encoders are rotating with pulley-belt systems. According to the ratio of pulley transmission (25 for the principal axis and 4 for secondary axis) the resulted angle precision is $0.014°$ for θ and $0.088°$ for β. Due to the belt strain, an approximate error of $0.2°$ is estimated for β angle (for θ angle, the belt is always tightened because SHIVA is always rotating in the same direction).

A 12-channels slip ring is used to transfer measurement signals from the blade load-cell to the triangular frame and an other 32-channels slip ring is used to transfer signals and power of embedded devices from rotating triangular frame to the outer frame and vice versa.

A Labview code allows users to synchronize collected measurements and set the parameters for capture data as sampling time and duration of acquisition.

2.3. Electrical Description
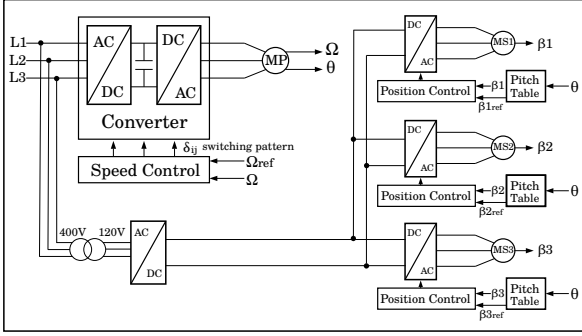### 2.3.1. Macro Overview

Figure 6: Electrical Diagram of the command architecture

The particularity of SHIVA lies on its electrical blade-control system which allows a wide range of pitch law investigation. As mentioned previously, SHIVA is composed of four permanent magnet synchronous machines (PMSM) (Figure 6), one for the main rotation and one for each blade. The main PMSM (MP), which provides the rotational speed, is alimented by a back to back converter powered by the 400V Alternative Current network from the IFREMER. The MP speed is controlled by a servo drive controller, TUBA series from Elmo brand (TUBA12/460R), which regulate the speed Ω of the MP in regards to the reference speed Ω_{ref}. The speed control is done by two Proportional-Integral (PI) controller strategies (one for the speed Ω and one for the current) which are used by default for the TUBA servo drive controller.

This main axis is supervised by a LabVIEW code through a Computer-Human Interface (CHI) which allows users to set the reference speed of SHIVA. This CHI communicates through a controller area network (CAN bus) with the TUBA, which is installed in an electrical cabinet alongside the IFREMER tank, and the MP at the top of SHIVA.

Another network 120V Direct Current is creating through a transformer and a rectifier also installed inside the electrical cabinet from the 400V AC (Figure 6). Then this network powers the three secondary PMSM (MS1, MS2, MS3) which rotating the blades through an embedded inverter for each secondary axis (the main slip ring is used to transfer power from the electrical cabinet to SHIVA). MSi are controlled in position by digital servo drives, CELLO series from Elmo brand (CEL-A15/200R). The position of the blade is the oriented angle between the main rotation tangent and the blade chord and referred β. Three PI controllers for each MSi are used: one for current, one for pitch rate $\dot{\beta}_i$ and one for pitch angle β_i. The pitch reference $\beta_{i_{ref}}$ is tabulated in function of the orbital position θ_i of each secondary axes. These tabulated functions are referred as pitch laws. One of

the special capacity of SHIVA is that each blade can follow a particular pitch law that procures a wide flexibility and range of investigation. Thanks to a second CHI, these pitch laws can be loaded even during the rotation.

2.3.2. Specific Description of Blade-control

Contrary to the main axis, blade pitch control system is embedded on SHIVA. In-house tests and developments over the past two years have involved the installation of an embedded Micro-Controller Unit (MCU) to dramatically boost the responsiveness of the system in comparison with a external computer. This MCU, a CompactRIO system from National Instruments, is divided into two entities : a Real Time computer module (RT) which executes LabVIEW Real-Time applications and offers multi-rate control, execution tracing and communication with peripherals ; associated with a user-programmable FPGA module which excels at smaller tasks that require high-speed logic and precise timing.

Figure 7 shows the classic blade-control used for SHIVA. The position loop is executed into the MCU for each secondary axis and then speed and current loops are executed by CELLOs which are chained on SHIVA. The advantage of moving the position control from the industrial CELLO to the MCU is to be able to modify PI parameters in real time to have an accurate control under various kinematics conditions.

Pitch laws are tabulated into the RT which holds a large memory space. For each blade-control iteration, pitch reference β_{ref} is given according to the blade orbital position θ. Because of the use of embedded system, an incremental rotary encoder is mounted on the triangular frame to measure this orbital position of SHIVA during the rotation and send the information directly to the MCU. Real pitch angle feedback, β, is also given by incremental rotary encoders mounted on each blade shaft. All these encoders are actuated by belt pulley system.
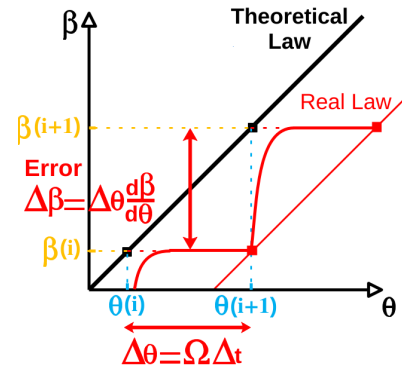

Figure 8: Schematic Error of Blade-control

The use of this PI controller strategy leads to a systematic error of pitch angle. Figure 8 illustrates this blade-control error for the case of a linear theoretical law (for example the case of the circular translation, $\beta = -\theta$, the blade is always parallel to the incoming flow). For each blade-control itera-
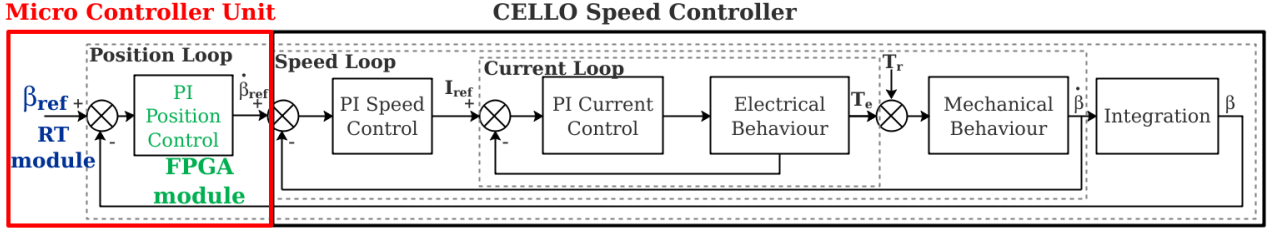
Figure 7: Diagram of Position Loop Control

tion, the controller will search into the tabulated law the new reference pitch angle $\beta_{ref}(i)$ for the considered orbital position $\theta(i)$. And between two iterations, the blade holds this position until the new position. This causes a systematic delay of the real position $\Delta\beta = \beta(i+1) - \beta(i)$ which depends on:

- The complexity of the pitch law $\frac{d\beta}{d\theta}$: more the derivative is sharp and more the error is high

- The rotational speed Ω : the angular step $\Delta\theta$ between two iterations depends on Ω for a given time step

- The time step Δt : sampling time of the regulation loop (time between two iterations)

Figure 8 illustrates the error in a case of a linear pitch law (such as trochoidal mode, the blade rotates between 0° and 360° in order to keep the leeding edge parallel to the incoming flow). For the case of a law in epicycloidal mode, the reference oscillates around $\beta=0°$. Hence the error fluctuates between delay or advance according to the derivative $d\beta/d\theta$ sign.

Because pitch laws are stored in the RT module, the regulation loop is limited by its sampling time which is around 2ms. The table below gives angular steps $\Delta\theta$ in function of rotational speed for $\Delta t=2$ms:

Ω (RPM)	10	20	30	40
$\Delta\theta$ (°)	0.12	0.24	0.36	0.48

Given the derivative ratio $d\beta/d\theta$ (which mostly depends on the orbital position) for an arbitrary pitch law and the rotational speed, this systematic error can be then estimated. Another delay of the real pitch control occurs when the pitch acceleration is higher than the capacities of auxiliary engines. In particular, for some pitch laws in epicycloidal mode (where the rotation is higher than trochoidal mode), acceleration limits of engines are reached during some period of the law. Next section illustrates these points by giving results of pitch tracking for various pitch laws under different kinematic conditions.

2.3.3. Pitch Tracking validation

The following results of pitch tracking have been computed from in-water measurements. The aim was to test various pitch laws for both kinematic cases, epicycloidal mode ($\lambda<1$) and trochoidal mode ($\lambda>1$). The flow velocity is set at 1.2 m/s for trochoidal laws and 0.8 m/s for epicycloidal laws

and rotational speed is calculated to reach desired λ value. Real pitch is recorded from rotary encoder and then phase-averaged over 30 rotation periods. The mean pitch is compared to the input reference law over one period.

For trochoidal mode, φ pitch angle is shown instead of β angle for a simpler viewing. φ is the oriented angle between the x-axis (flume tank direction) and the blade chord.

Figure 9 shows pitch tracking for three trochoidal laws. The circular translation (Figure 9-a) is defined as the blade leading edge is always parallel to the tank flow direction (i.e. $\varphi=0$ or $\beta=-\theta$). For this law, the rotational speed is set at 28.6 RPM. A low constant delay is observed just under 0.4° which is due to the systematic error shown previously. The real pitch is always late compared to the reference. The standard deviation shows a uniform distribution of the real pitch over orbital positions for all the different laps (here the pitch angle is close to 0 compared to other figures, it is why the deviation seems wide).

The sinusoidal pitch law with 20° amplitude (Figure 9-b) is well tracked with a satisfying maximal error under 1°. This maximal error occurs at the position $\theta=120°$ and is correlated to the manifestation of the highest measured hydrodynamic load. Indeed hydrodynamic forces involve pressure on blades that makes the reference law more difficult to follow. The standard deviation shows a low dispersion over the measurement laps.

The third pitch law (Figure 9-c) refers to a kinematic process of optimization [16] in trochoidal mode used to boost the efficiency of the system for complex law. This law presents some quick transitions which lead to an increasing tracking error (for θ between 340° and 20° and θ around 180°) but globally the blade is closely following the reference even if the rotational speed is higher than for the sinusoidal case.

Figure 10 shows pitch tracking results for epicycloidal mode. For the case of the 0-pitch law (Figure 10-a), the set-point is zero for all orbital positions : the blade stays parallel to the main rotor disk (it's the case for no-pitch system as Darrieus turbines in marine energy domain). The blade is well following the reference with a maximal error around 0.6°. This error oscillates around 0 because of the changeable relative flow direction over the orbital position. Again the standard deviation seems high here because of the closeness of the pitch law to 0, but it shows a uniform dispersion over orbital positions.

Figures 10-b and 10-c refer to two epicycloidal pitch laws which was again optimized by a kinematic process [16]. For
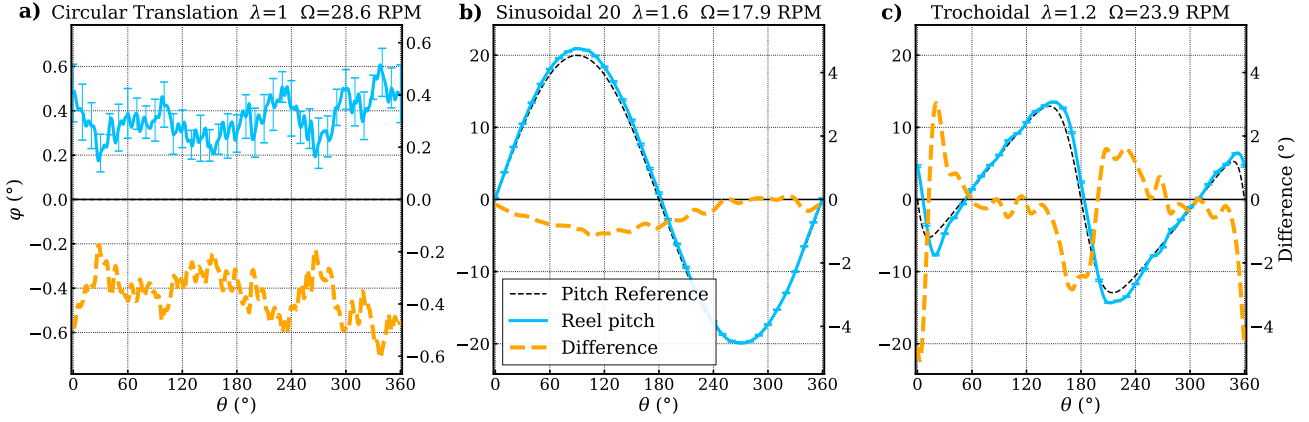
Figure 9: Pitch tracking in trochoidal mode for **a)** Circular Translation λ=1 pitch law; **b)** Sinusoidal 20deg λ=1.6 pitch law; **c)** Trochoidal λ=1.2 pitch law. Blade pitch angle φ on the left axis and difference between real and reference pitch on the right axis
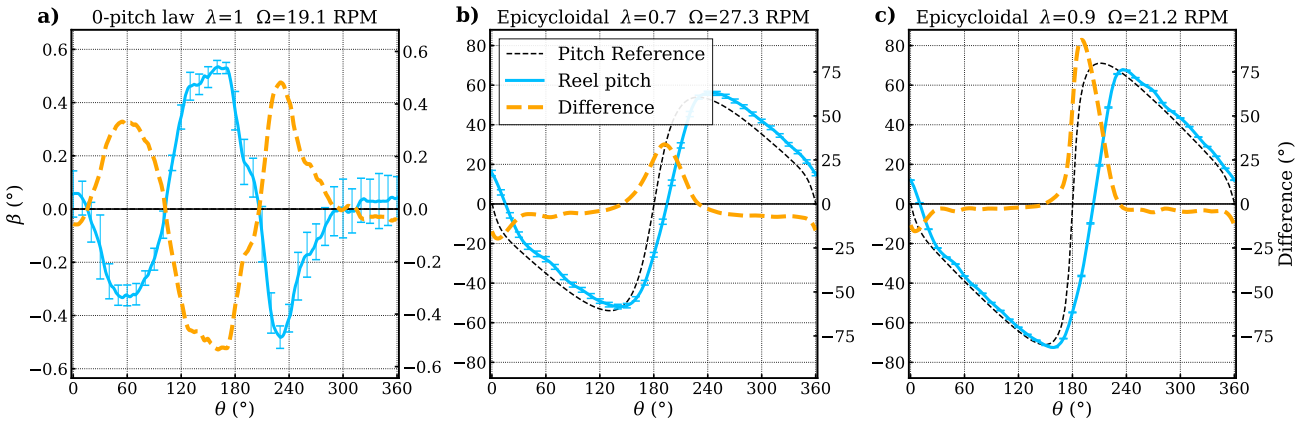

Figure 10: Pitch tracking in epicycloidal mode for **a)** 0-pitch law for λ=1; **b)** Epicycloidal λ=0.7 pitch law; **c)** Epicycloidal λ=0.9 pitch law. Blade pitch angle β on the left axis and difference between real and reference pitch on the right axis

these laws, blades are reversing at θ=180° (β switch from negative to positive value) that induces a high acceleration to servo-motors. The pitch tracking is thus less accurate during this blade reversal. The difference is even higher for the case of λ=0.9 pitch law because of the quicker reversal than λ=0.7 pitch law. Fortunately this is not during this reversal blade movement that the blade generates the higher hydrodynamic thrust.

In case of λ=0.7 (Figure 10-b), the rotation speed is higher than in case of λ=0.9 for the same flow speed (due to the definition of λ). This leads to a higher systematic error during the soft motions phases of the blade ($\theta \in$ [30:150] and [210:330]). For both cases, standard deviation shows again a well repeatability over measurement laps.

These results show an accurate blade pitch tracking for trochoidal case whereas a higher tracking error is observed for epicycloidal mode essentially due to the reversal blade phenomenon and higher rotational speed. Indeed the use of servo-motors for blade pitching allow the propeller to run various pitch laws but is also subject to the main following limitations:

- Servo-motors speed and acceleration limits involve restrictions on the pitch curve shape and the derivative $d\beta/d\theta$

- Blade control strategy which implicates a systematic error that depends on the rotational speed Ω and the sampling time of regulation loop Δt

Nevertheless, presence of rotary encoders provides the real pitch feedback for both real time tracking and post-process procedure. The control-CHI also allows users to adjust both PI parameters (K_I, K_P) in the position loop in order to adapt the reactivity of blade-control and thus reduce the tracking error.

To decrease the systematic error, ongoing developments are undertaken to reduce the sampling time of regulation loop by saving reference pitch laws into the FPGA module which is sampled at 0.05 ms and hence reduce the orbital step $\Delta\theta$ between two regulation iterations for a same rotational speed. However, classical PI controller strategy is not the most suitable method for fluctuating pitch law. Here the industrial speed controllers (CELLO and TUBA) use this method of blade control but a new strategy using non linear controllers

could be investigated, even though this area of work is out of scoop for the moment.

3. Cross-flow propeller prototype efficiency

This last section presents results from in-water measurements for sinusoidal pitch laws with three different amplitudes in the trochoidal mode. Experimental setup and post-process are first presented then results are discussed.

3.1. Experimental setup and Post-process procedure

First, in-air measurements are used to eliminate centrifugal effect from the embedded load-cell measurements and mechanical internal resistance on the main torque sensor. Then measurements in the tank without flow velocity and rotation are carried out to remove buoyancy effects and pre-stress of fixed load-cell. These static measurements are done for a range of orbital positions ($\theta \in [0, 360, 30]$) and pitch angles ($\beta \in [0, 360, 30]$). Because the variation of voltages doesn't exceed 5% as shown in Figure 11, the mean value is calculated and subtracted to the in-flow measurements. This step is repeated everyday, only for orbital positions, to ensure any unexpected behaviour.
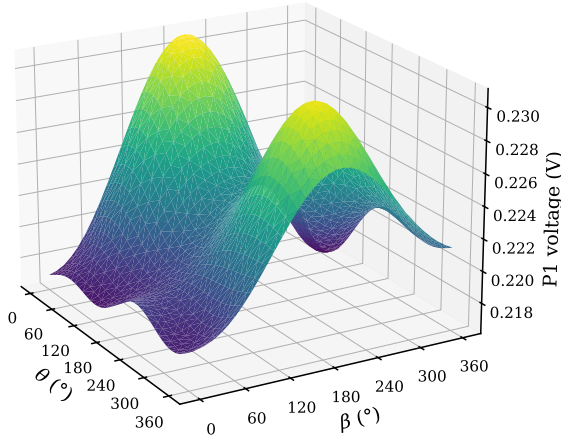
Figure 11: Representation of P1 Voltage of the embedded load-cell for the static measurements over 360° in θ and β

A mechanical verification of each blade position β_i and the position of the main axis θ is done before starting the flow motion to ensure that recorded angles correspond to the real positions of motors. In-flow measurements are launched after waiting that the flow is well established at V=1.2m/s and the wake is stabilized with the rotational speed of SHIVA and the chosen pitch motion. K_I and K_P parameters are eventually adjusted to guarantee an accurate pitch tracking. Temporal signals are then recorded over 30 rotation periods. Because of the electromagnetic environment mainly caused by Pulse Width Modulation (PWM) of speed controllers, these temporal signals are perturbed by high frequencies. A low-pass filter (cut frequency of 30Hz) is applied on temporal signals.

Temporal voltages are then transformed to loads thanks to the transfer matrix. Pitch and orbital angles are used to convert local hydrodynamic loads from the embedded load-cell to global forces given by equations (2) and (3).

$$\begin{pmatrix} F_T \\ F_N \end{pmatrix} = \begin{pmatrix} \cos(\beta) & -\sin(\beta) \\ -\sin(\beta) & -\cos(\beta) \end{pmatrix} \begin{pmatrix} F_{Tb} \\ F_{Nb} \end{pmatrix} \quad (2)$$

$$\begin{pmatrix} F_X \\ F_Y \end{pmatrix} = \begin{pmatrix} \cos(\theta) & \sin(\theta) \\ -\sin(\theta) & \cos(\theta) \end{pmatrix} \begin{pmatrix} F_T \\ F_N \end{pmatrix} \quad (3)$$

All the load are then phase-averaged over all the periods as shown in Figure (12). Mean and standard deviation are calculated for each of the load signals.
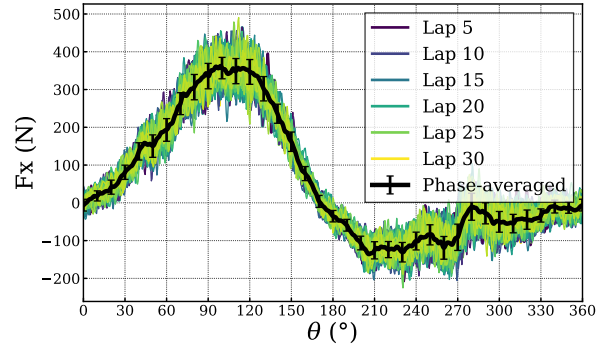
Figure 12: Phase-average operation over 30 periods for the Thrust signal in the case of the 20° sinusoidal pitch law for λ=1.2 and V=1.2m/s

Finally, as the embedded load-cell measures the hydrodynamic force on only one blade, mean-averaged loads are shifted of $\frac{\pi}{3}$ and $\frac{2\pi}{3}$ and added to construct the total hydrodynamic loads acting on all the three blades. By making this operation, it is assumed that all blade has the same pitch tracking. The four fixed load-cells signals are also summed up to yield the total forces applied on the fixed frame. Dimensionless force coefficients are given by equations (4) where F is a hydrodynamic force and T a torque:

$$C_F = \frac{F}{0.5 \rho S V^2} \quad C_T = \frac{T}{0.5 \rho S D V^2} \quad (4)$$

Where S is the swept frontal area ($S = Dl$) and V the flume tank flow velocity.
Hydrodynamic efficiency is lastly defined as:

$$\eta = \frac{\overline{Fx_{tot}} \, V}{\overline{C_{tot}} \, \Omega} \quad (5)$$

Where $\overline{Fx_{tot}}$ and $\overline{C_{tot}}$ are respectively the mean of total Thrust and total Torque over 360°.

3.2. Sinusoidal pitch results

Post-process procedure is adopted on a 20° sinusoidal pitch law measurements at V=1.2 m/s and Ω=23.88 RPM
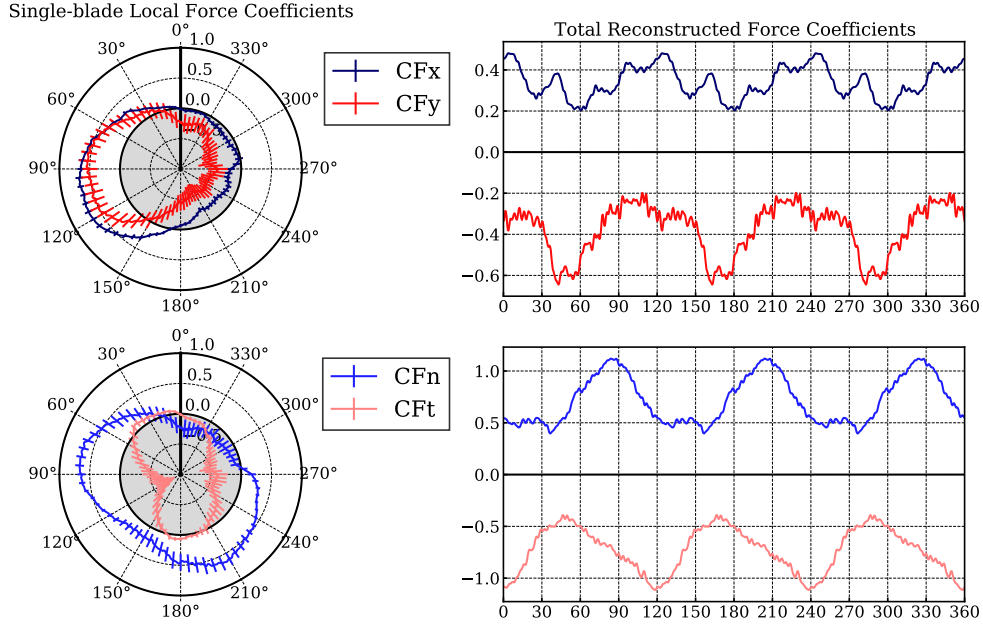
Figure 13: Single-blade Force coefficients at the left and Reconstructed total Force coefficients at the right for the case of the 20° sinusoidal pitch law for λ=1.2 and V=1.2m/s

(corresponding to λ=1.2), for which the local Reynolds number, $Re = \frac{cV}{\nu}$, is around 420 000.

Figure 13 gives single-blade force coefficients on the left and total reconstructed coefficients on the right. As shown on the polar plot, maximal thrust and side force are generated for θ between 90° and 120°. In the wake, thrust tends toward zero and becomes even negative while side force reverses. The total reconstructed thrust is always positive with some fluctuations while total side force is still negative, the wake is deflected on the tank side. This observation on the wake deflection is explained by the fact that for cycloidal propulsion the hydrodynamic center of thrust is not aligned with the rotor center.

For the normal and tangential coefficients, the distribution over orbital positions is quite different. Normal force is almost always spread outwards the rotor with two maximum at θ=70° and θ=210° while tangential force is almost always negative with two maximum at θ=120° and θ=270°. As the total tangential coefficient is still negative, this proves that generated hydrodynamic force counters the rotation of the main motor with fluctuations which can provoke damages. So the propeller needs to provide a torque to generate the desired thrust.

Figure 14 presents the comparison between reconstructed force coefficients from the embedded load-cell and the measurements from fixed load-cells and the torque sensor. Mean values over 360° are represented by a short line at the left of each figure. Even if fixed sensors and embedded load-cell seem to measure the same global behaviour of the propeller,

mean values over the period are slightly different. That implies a strong disparity on the hydrodynamic efficiency if it is expressed by fixed sensors or by embedded load-cell measurements.

These differences are mainly explained by the fact that embedded and fixed load-cells have a large measurement range (-5000N to 5000N) in comparison with measured hydrodynamic loads (-100N to 400N). For this reason, the flow velocity has been set at 1.2 m/s and blade chord has been increased with the addition of the epoxy-fiberglass shells to raise hydrodynamic loads.

This loads increasing causes a shaking of all the frame during the rotation of the propeller. This shaking is observed by fixed load-cell as shown large fluctuations on frame signals in Figure 14. It is also the case of the torque sensor which measures these oscillations on the main axis. But this shaking seems to be less detected on the instrumented blade. Embedded load-cell underestimates the total hydrodynamic loads. A new embedded load-cell with a smaller measuring range (±900N for normal blade direction and ± 400N for tangential blade direction) is currently manufactured to remedy this problem.
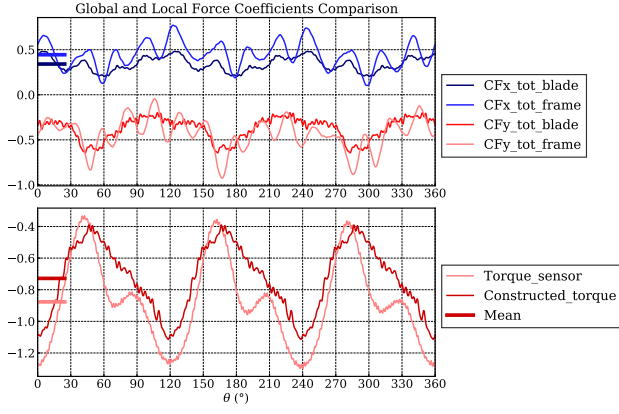
Figure 14: Comparison of blade reconstructed force coefficients and frame sensor force coefficients for the case of the 20° sinusoidal pitch law for λ=1.2 and V=1.2m/s

For the presented results, hydrodynamic efficiency is thus expressed using the mean of the total frame thrust divided by the mean of the torque sensor instead of the blade embedded load-cell measurements to take care about the true solicitations of the experimental platform which are not detected by the embedded load-cell.

Measurements for other rotational speeds and other sinusoidal pitch laws are undertaken to determine the performance curve for sinusoidal pitch propeller. Figure 15 shows the results for sinusoidal pitch laws of 10°, 20°, 30° and 40° of maximal amplitude.
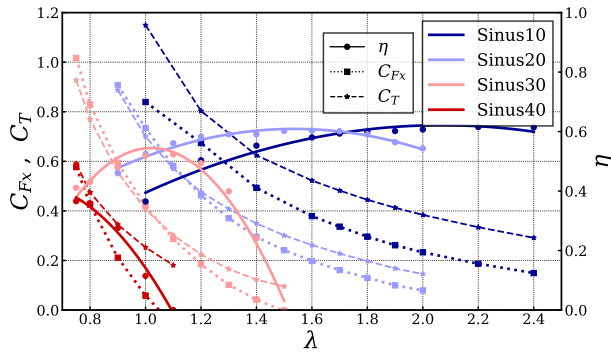

Figure 15: Efficiency and force coefficients versus advance parameter λ for 10°, 20°, 30°, 40° sinusoidal pitch laws at V=1.2m/s

Results reveal that for the presented propeller configuration, the Sinus40 law have the lower hydrodynamic efficiency which falls when the advance parameter exceed 0.8 value. This law isn't adapted to our configuration of solidity for an efficient purpose and for trochoidal mode. Then, depending of the value of the advance parameter, each other pitch law is interesting with a maximal efficiency reached for different values of λ. These results prove the need of adapting the pitch to the λ value. It also means that during ac-

celeration phase, it is preferable to start with high amplitude pitch law then decrease the pitch amplitude. Concerning the thrust, the Sinus10 law have the higher values for all advance parameters. It shows that for manoeuvre which requires high thrust, the pitch must be decreased, balancing a reduction of the efficiency. Lastly, theses results justify the use of vertical axis propeller with a variable pitch control system.

To go further, as perspective for next experiments, SHIVA will be used for experimental optimization purpose. Indeed, the complexity of the flow through cross-flow propeller implies a strong discrepancy between upstream and downstream halves. Hence, there is no reason why the pitch law definition should be symmetrical (as in case of most conventional cycloidal propeller).

The optimization procedure consists primarily to parameterize the pitch law with an appropriate method such as the one described by Abbaszadeh [1]. This method employs a spline generated through several control points, the parameters, which can evolve inside fixed ranges. This parameterisation allows asymetrical pitch generation. Parameters are then optimized using a Gaussian Process method developed by Sacher [25]. A Meta-model is then utilized to represent the objective function in parameters space. This objective function is calculated from in water measurements. Multiple-objective optimization could be done the determine the Pareto efficiency through the dual objectives: maximizing the thrust and the efficiency. By repeating this process for many λ values, optimal pitch laws will be established for various operation mode (low advance speed, cruising speed or transitional mode).

4. Conclusion and Perspectives

The experimental blade-controlled propeller designed at the Naval Academy Research Institute is presented in this study. Modular mechanical features allow comparisons for different solidity, Reynolds or aspect ratio numbers. The size of the system makes it ideal to test large-scale prototypes.

The technical progress published here is its electrical blade-control design which offers a huge range of pitch law investigations. Blade control/command is tested with in-house experiments comparing pitch reference and real pitch tracking. Even if results reveal a suitable tracking, some limitations due to the technology of speed controller are underlined. Indeed the use of regulation loop implies a systematic error which is hard to overcome. Using a more complex speed-control strategy could mitigate this error. Speed limitations of electric motors are also faced for high speed kinematics. As blade position angles are registered during acquisition of measuring signals, this position error is acceptable for our investigations. However, long-term upgrade of the control system is expected to improve the pitch tracking and the precision of angle measurements.

Post-process has been validated on sinusoidal pitch laws for trochoidal mode. Discrepancies on hydrodynamic measurements occurred between the blade embedded load cell and fixed load cells. These differences are mainly explained by

a strong stress of the frame due to the high velocities encountered. Next experiments will be carried on with more precise load sensor measuring ranges, so that flume tank velocity and rotational speed could be reduced to be no more subject to high solicitations of the platform.

Results exposed here show promising capacities of the platform in terms of propeller performance measurement. As perspective in the quest of the ideal pitch law and because the electrical blade-control system allows it, an experimental optimization procedure is intended for various advance parameter values.

References

[1] Abbaszadeh, S., Hoerner, S., Maître, T., Leidhold, R., 2019. Experimental investigation of an optimised pitch control for a vertical-axis turbine. IET Renewable Power Generation 13, 3106–3112.

[2] Bakhtiari, M., Ghassemi, H., 2020. Cfd data based neural network functions for predicting hydrodynamic performance of a low-pitch marine cycloidal propeller. Applied Ocean Research 94, 101981.

[3] Barrett, D., Triantafyllou, M., Yue, D., Grosenbaugh, M., Wolfgang, M., 1999. Drag reduction in fish-like locomotion. Journal of Fluid Mechanics 392, 183–212.

[4] Bartels, J.E., Jürgens, D., 2006. The voith schneider propeller: Current applications and new developments. Heidenheim: Voith Publication .

[5] Bose, N., 1987. Rotary foil propellers. Tokyo, Japan: Ship Research Institute, Ministry of Transport .

[6] Bose, N., Lai, P.S., 1989. Experimental performance of a trochoidal propeller with high-aspect-ratio blades. Marine Technology and SNAME News 26, 192–201.

[7] Consul, C.A., Willden, R.H.J., McIntosh, S.C., 2013. Blockage effects on the hydrodynamic performance of a marine cross-flow turbine. Philosophical Transactions of the Royal Society A: Mathematical, Physical and Engineering Sciences 371, 20120299.

[8] Delafin, P.L., Deniset, F., Astolfi, J.A., Hauville, F., 2021. Performance improvement of a darrieus tidal turbine with active variable pitch. Energies 14, 667.

[9] Epps, B.P., Roesler, B.T., Medvitz, R.B., Choo, Y., McEntee, J., 2019. A viscous vortex lattice method for analysis of cross-flow propellers and turbines. Renewable Energy 143, 1035–1052.

[10] Esmailian, E., Ghassemi, H., Heidari, S.A., 2014. Numerical investigation of the performance of voith schneider propulsion. American Journal of Marine Science 2, 58–62.

[11] Fasse, G., Bayeul-Lainé, A.C., Coutier-Delgosha, O., Curutchet, A., Paillard, B., Hauville, F., 2019. Numerical study of a sinusoidal transverse propeller, in: IOP Conference Series: Earth and Environmental Science, IOP Publishing. p. 052007.

[12] Ficken, N.L., Dickerson, M.C., 1969. Experimental performance and steering characteristics of Cycloidal Propellers. volume 2983. Department of the Navy, Naval Ship Research and Development Center.

[13] Gaurier, B., Davies, P., Deuff, A., Germain, G., 2013. Flume tank characterization of marine current turbine blade behaviour under current and wave loading. Renewable Energy 59, 1–12.

[14] Haberman, W., Harley, E., 1961. Performance of Vertical Axis (Cycloidal) Propellers Calculated by Taniguchi's Method. Technical Report. David Taylor Model Basin Washington DC.

[15] Halder, A., Walther, C., Benedict, M., 2018. Hydrodynamic modeling and experimental validation of a cycloidal propeller. Ocean Engineering 154, 94–105.

[16] Hauville, F., Lecuyer-Le Bris, R., Deniset, F., Fasse, G., 2018. Pitch law optimization of a cycloidal propulsor, in: 16e Journées de l'Hydrodynamique, Marseille, France.

[17] Hu, J., Li, T., Guo, C., 2020. Two-dimensional simulation of the hydrodynamic performance of a cycloidal propeller. Ocean Engineering 217, 107819.

[18] Ikhennicheu, M., Germain, G., Druault, P., Gaurier, B., 2019. Experimental study of coherent flow structures past a wall-mounted square cylinder. Ocean Engineering 182, 137–146.

[19] Kirsten, J., 1922. Propeller. US Patent 1432700. URL: https://patents.google.com/patent/US1432700.

[20] van Manen, J.D., 1966. Results of systematic tests with vertical axis propellers. International Shipbuilding Progress 13, 382–398.

[21] Mendenhall, M.R., Spangler, S.B., 1973. Theoretical Analysis of Cycloidal Propellers. Part II. Program Manual. Technical Report. Nielsen Engineering and Research Inc Mountain View California.

[22] Nakonechny, B.V., 1974. Design of a 9-inch cycloidal propeller model unit and some experimental results. Technical Report.

[23] Paillard, B., Astolfi, J.A., Hauville, F., 2015. Uranse simulation of an active variable-pitch cross-flow darrieus tidal turbine: Sinusoidal pitch function investigation. International Journal of Marine Energy 11, 9–26.

[24] Roesler, B.T., Kawamura, M.L., Miller, E., Wilson, M., Brink-Roby, J., Clemmenson, E., Keller, M., Epps, B.P., 2016. Experimental performance of a novel trochoidal propeller. Journal of Ship Research 60, 48–60.

[25] Sacher, M., Hauville, F., Duvigneau, R., Le Maître, O., Aubin, N., Durand, M., 2017. Efficient optimization procedure in non-linear fluid-structure interaction problem: Application to mainsail trimming in upwind conditions. Journal of Fluids and Structures 69, 209–231.

[26] Schneider, E., 1928. Blade wheel. US Patent 1681500. URL: https://patents.google.com/patent/US1681500.

[27] Sparenberg, J., 2002. Survey of the mathematical theory of fish locomotion. Journal of Engineering Mathematics 44, 395–448.

[28] Sparenberg, J., De Graaf, R., 1969. On the optimum one-bladed cycloidal ship propeller. Journal of Engineering Mathematics 3, 1–20.

[29] Taniguchi, K., 1962. Sea trial analysis of the vertical axis propellers. Mitsubishi Heavy Industries Ltd, Mitsubishi Technical Bulletin No. 6 .

[30] Triantafyllou, M.S., Techet, A.H., Hover, F.S., 2004. Review of experimental work in biomimetic foils. IEEE Journal of Oceanic Engineering 29, 585–594.

[31] Zhu, D., 1981. A computational method for cycloidal propellers. International Shipbuilding Progress 28, 102–111.